

2. Optical constants of 5CB and E7 (nematic liquid crystals) in terahertz frequency range

2.1. Introduction

The knowledge of the frequency dependence and the magnitude of the refractive indices as well as the birefringence ($\Delta n = n_e - n_o$) of liquid crystals (LCs) is a key parameter for both fundamental studies and practical applications of LCs. Many groups have investigated the birefringence of LCs in the visible [1-5]. In the infrared, the refractive indices and other optical properties of LCs have also been reported [6-9]. In the millimeter wave range, Lim *et al.* [10] first showed that many LCs have comparatively large birefringence with approximate values in the of 0.1-0.18 range at 30 GHz. Further, the birefringence of LCs varied only slightly in the 15-94 GHz range. Based on this, liquid-crystal-based waveguide-type or microstrip-type phase shifters in millimeter wave regions have been demonstrated [10-12]. In the submillimeter wave range, the refractive indices and transmission losses for some nematic LCs, including 4'-*n*-pentyl-4-cyanobiphenyl (5CB), have been measured by Nose *et al.* [13] at three discrete wavelengths (118, 215, and 435 μ m): The refractive indices of 5CB for ordinary (n_o) and extraordinary rays (n_e) in the submillimeter wave region were found to be slightly larger than those in the visible range. A large birefringence comparable to that in the visible range was also reported. For mixture LC, E7, Yang and Sambles [14], for example, reported $n_e = 1.793$, $n_o = 1.647$ in the 26.0 – 40.0 GHz region. The same authors reported $n_e = 1.782$, $n_o = 1.654$ or $\Delta n=0.128$ in the 50.0–75.0 GHz region [14] and $\epsilon_e = 3.17$ ($n_e = 1.78 \pm 0.01$) and $\epsilon_o = 2.72$ ($n_o = 1.65 \pm 0.01$), ($\Delta n \sim 0.13$) in the 40.0 –

60.0 GHz region [15]. A range of values, between 0.11 and 0.19 for E7 at 30 GHz, were reported in earlier works [16-18].

Although many groups concerning the near-IR or GHz range, we can expect a large birefringence with a low loss similar to that in visible range, the optical constants in THz frequency range still wasn't reported completely. It is attractive for the quasi-optic THz application field. In the IR wavelength region, however, there are usually many absorption bands in LCs. In wavelength as long as 50 μm , the absorption properties have been thoroughly investigated with spectrometers, but only a few experimental results on the refractive indices and optical properties have been reported in this region.

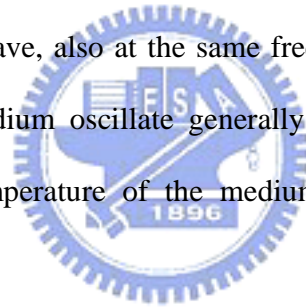
In this chapter, we report the complex optical constants of 5CB by using THz time-domain spectroscopy to determine it. In Sec.2.2, the theory of refractive indices of nematic LC and the numerical method employed in this work will be introduced. The sample preparation about cells and temperature controlled system will be shown in Sec.2.3. The measured results and discussion are in the Sec.2.4 and Sec.2.5. Then we will summary this work in Sec.2.6.

2.2. Theory

2.2.1. Refractive indices of nematic liquid crystal

When a dielectric is introduced into an electric field, its constituent molecules, in general, become polarized and tend to line up with the resultant field [19]. For normal gases and liquids the dielectric constant correlates with mean molecular polarizability and is described by the well-known Clausius-Mossotti equation at low frequencies [20].

Wu has also demonstrated the three-band model for the refractive index dispersions of nematic LCs successfully [19]. The model can fit the indices of refraction quite well with known absorption band near/in the probed frequency range. However, the known absorption bands are necessary for using this model. Presently, the refractive indices of LCs in THz range are not carried out completely and there is no observed resonant absorption so far, which means that it cannot be employed in the THz regime. For liquids whose molecules have dipole moments, the low frequency dielectric constant is usually much greater than the corresponding value at optical frequencies. At optical frequencies, the electric field of the incident electromagnetic wave causes the induced dipoles to oscillate at the same frequency. The resultant motion of charge, in turn, re-emits an electromagnetic wave, also at the same frequency. The efficiency with which the dipoles of a given medium oscillate generally varies with the frequency of the incident wave and the temperature of the medium, resulting in dispersions of the refractive index.



Nematic liquid crystals (NLCs) consist of rodlike molecules, which tend to line up with each other. The thermal average of the molecules orientation is called the director. The dielectric constants are anisotropic. When a linearly polarized monochromatic light wave propagates through a aligned LC cell with its polarization having an angle (except 0° and 90°) to the director, the extraordinary and ordinary rays in the outgoing light experience a phase difference due to the different propagating speeds in the LCs. The optical anisotropy, so-called birefringence ($\Delta n = n_e - n_o$, where the n_e and n_o are the refractive indices for the extraordinary and ordinary rays, respectively), is large and can be controlled by an external field. Many electro-optical devices employing LCs take the

advantage of the fact that a significant phase change can be accomplished by a reasonable low voltage. Examples are a LC-based tunable phase retardation plate, a LC light switch, a photo-activated LC spatial light modulator, and LC displays [6,21-23]. For those applications, the temperature and frequency dependent indices of refraction are particularly important. In visible frequency range, the optical constants of many LCs have been well investigated. These results brought up many applications quite successfully. The measured optical constant in THz range is the first step to use LCs for the quasi-optical devices and applications in this range.

2.2.2. Determination of optical constants

For the optical constant measurement, we prepared two cells, the reference cell and the LC cell. The reference cell is constructed by two fused silica substrates contacting with each other (See Fig.2.2.2.1 (a)). The LC cell is constructed by two fused silica substrates separated by 250- μm Mylar spacer and filled with 4'-*n*-pentyl-4-cyanobiphenyl (5CB, Merck) as shown in Fig.2.2.2.2(b). The inner surfaces are coated polyimide films, which are baked and rubbed to give LCs the homogeneous alignments.

Assuming a plane wave passing through the cell normally, the electric field of the THz wave transmitted through the reference cell at angular frequency, ω , can be written as

$$E_{reference}(\omega) = E_0(\omega) \cdot \eta(\omega) \cdot P_{air}(\omega, d), \quad (2.2.2.1)$$

where $E_0(\omega)$ is the electric field of THz wave before passing through the cell, $\eta(\omega)$ is a coefficient including all the reflection, transmission and propagation coefficients in

fused silica and $P_{air}(\omega, d)$ is the propagation coefficient in air, which the d is the thickness of the LC layer. In general, for a medium a over a distance L , the propagation coefficient $P_a(\omega, L)$ can be written as $\exp[(-i\tilde{n}_a\omega L)/c]$, where \tilde{n}_a ($\tilde{n}_a = n_a - i\kappa_a$) is the complex refractive index of medium a , which depends on the wave frequency. In $\eta(\omega)$, the echoes of the THz wave or the Fabry-Perot effect in fused silica are neglected because that these signals are far away from the main signal on time domain and will be truncate during the frequency spectrum analysis. The electric field of the THz wave passing through the LC cell is given by

$$E_{LC}(\omega) = E_0(\omega) \cdot \eta(\omega) \cdot T_{q-LC}(\omega) \cdot P_{LC}(\omega, d) \cdot T_{LC-q}(\omega) \cdot F_{LC}(\omega, d), \quad (2.2.2.2)$$

where $T_{i-j}(\omega)$ is the transmitted Fresnel factor of $i-j$ interface, which is $T_{i-j}(\omega) = (2 \cdot \tilde{n}_i) / (\tilde{n}_i + \tilde{n}_j)$ and $F_a(\omega, L)$ is the Fabry-Perot effect in medium a with the thickness of L . The $\eta(\omega)$ for the LC cell is the same as for the reference cell, because of we have chosen the fused silica substrates with same thickness (tolerance $< 2\mu\text{m}$). The complex transmission coefficient $T(\omega)$ of the measured LC can be obtained by dividing the LC signals, $E_{LC}(\omega)$, by the reference signals, $E_{reference}(\omega)$, as follow

$$T(\omega) = \frac{E_{LC}(\omega)}{E_{ref}(\omega)} = \frac{4 \cdot \tilde{n}_{LC} \cdot \tilde{n}_q}{(\tilde{n}_{LC} + \tilde{n}_q)^2} \cdot \exp\left[-i(\tilde{n}_{LC} - \tilde{n}_{air}) \frac{\omega \cdot d}{c}\right] \cdot F_{LC}(\omega), \quad (2.2.2.3)$$

where \tilde{n}_q is either the complex index of fused silica and \tilde{n}_{LC} is the ordinary indices ($\tilde{n}_o = n_o - i\kappa_o$) or extraordinary indices ($\tilde{n}_e = n_e - i\kappa_e$), which can be detected by ordinary ray (the polarization of the THz wave is perpendicular to the orientation of the LC molecules) or extraordinary ray (the polarization of the THz wave is parallel to the

orientation of the LC molecules). Duvillaret *et al.* have demonstrated the solutions in 1996 both for optically thick and thin samples [24]. The optically thick sample means that the echoes of THz waves from the multiple reflections of sample are temporally well separated from the main signal, which passes through the sample directly without any reflection from interface. So the $F(\omega)$ in Eq. 2.2.2.3 can be removed or equal to 1. On the other hand, the $F_{LC}(\omega)$ cannot be ignored in optical thin case, which is

$$F_{LC}(\omega) = \frac{(\tilde{n}_{LC} + \tilde{n}_q) \cdot \exp(-2i\tilde{n}_{LC}\omega d/c)}{(\tilde{n}_q - \tilde{n}_{LC}) \cdot (\tilde{n}_{LC} - \tilde{n}_q)}. \quad (2.2.2.4)$$

If we let the reference cell have a empty gap of the same thickness of LC cell, the $F(\omega)$ will be rewritten as

$$F(\omega) = \frac{(\tilde{n}_q - \tilde{n}_{air}) \cdot (\tilde{n}_{air} - \tilde{n}_q) \cdot (\tilde{n}_{LC} + \tilde{n}_q) \cdot \exp(2i(\tilde{n}_{LC} - \tilde{n}_{air})\omega d/c)}{(\tilde{n}_q - \tilde{n}_{LC}) \cdot (\tilde{n}_{LC} - \tilde{n}_q) \cdot (\tilde{n}_{air} + \tilde{n}_q)}. \quad (2.2.2.5)$$

Instead of solving \tilde{n}_{LC} from $T(\omega) - T_{meas}(\omega) = 0$, where $T(\omega)$ and $T_{meas}(\omega)$ are respectively the calculated and measured complex transmission coefficients, we define an error function, $\delta(n, \kappa)$, and then find (n, κ) by minimizing the error function. The error function is defined as following:

$$\delta(n, \kappa) = \delta\rho^2 + \delta\varphi^2 \quad (2.2.2.6)$$

where

$$\delta\rho = \ln(|T(\omega)|) - \ln(|T_{meas}(\omega)|) \quad (2.2.2.6a)$$

$$\delta\varphi = \arg(T(\omega)) - \arg(T_{meas}(\omega)) \quad (2.2.2.6b)$$

For minimizing the error function, we use Nelder-Mead method [25] by building a program in MatLab. Briefly, the Nelder-Mead method is a simplex method for finding a local minimum of a function of several variables. For two variables (our case) and the method is a pattern search that compares function (in our case is error function) values at three vertices of a triangle. The worst vertex, where the value of the function is largest, is rejected and replaced with a new vertex. A new triangle is formed and the search is continued. The process generates sequence triangles (which might have different shapes), for which the function values at the vertex get smaller and smaller. The size of the triangles is reduced and the coordinates of the minimum point are found.

If the sample is optically thin, which means the echoes are too close to the first directly transmitted THz pulse and cannot be cut off at a nonzero value. The Fabry-Perot effect should be considered in this case, which is more complex than thick one. To record all successive echoes of THz signals needs a very large temporal scale and has to avoid the reflection signals from substrates. The different situations of the thin sample have been discussed already. The minimum of the error function, $\delta(n, \kappa)$, is difficult to be found with considering the Fabry-Perot item, $F(\omega)$, in Eq. 2.2.2.3 by using the mentioned method. The approximate n and κ can be obtained without $F(\omega)$ easily and used to estimate the value of $F(\omega)$. After dividing the measured complex transmission coefficient, $T_{meas}(\omega)$, by the estimated $F(\omega)$, we can obtain the modified transmission coefficient (Eq. 2.2.2.3) with the Fabry-Perot effect deduced by estimated value. Then

we repeat the procedure by using modified coefficient instead of measured coefficient several times till the indices, n and κ , are obviously unchanged.

2.3. Sample preparation

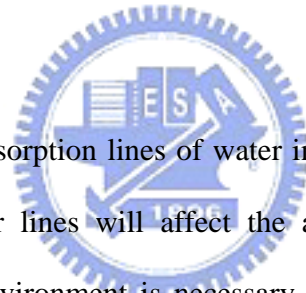
2.3.1. Liquid crystal cell and reference cell

Two cells, reference cell and homogeneous liquid crystal cell, were prepared in this work shown in Fig. 2.2.2.1. The reference cell was constructed by two fused silica windows, which contact to each other. The nominal thickness is 3000 μm each. The polyimide film was spin coated on inner surface in order to obtain the similar condition with liquid crystal cell. For liquid crystal cell, the measured liquid crystal, commercial available 5CB (Merck), was sandwiched by two fused silica windows. The nominal thickness of these two fused silica window is 3000 μm . The thickness of liquid crystal layer was controlled with Mylar spacer and measured by interference method with 260 μm . The tolerance of the thickness between the two inner surfaces of substrates in measured area is less than 3 μm . The homogeneous alignment is achieved by coating polyimide on inner surfaces of substrates and rubbing it. The measured pretilt angle is about 1 degree [26]. The liquid crystal cell was mounted in a copper oven for the stable temperature control.

2.3.2. Temperature and humidity controlled system

In order to obtain the temperature dependence of the LCs' refractive indices, an accuracy temperature controlled system is necessary. We put the cell in a copper box, which has two open windows for THz wave passing. The copper box was covered by Teflon with the thickness of 0.5cm for keeping the temperature inside. The copper box

also has two small holes with the diameter of 3.0 mm for resistant type temperature probes (YSI 423, Yellow Springs Instrument Co., Inc.) and two larger holes with 1.0-cm-diameter for cylinder current heaters. One of the probe and two heaters were connected to a temperature controller (YSI Model 72, Yellow Springs Instrument Co., Inc.) in order to set the temperature of the cells. Another probe, which directly contacts the cell was connected to a voltage multimeter for probing the actual cell temperature by reading the resistance of the probe. Figure 2.3.2.1 shows the pictures of the temperature controlled sample holder. The fluctuation of the temperature of the cell is less than 0.04°C . The testing data is shown in Fig. 2.3.2.2. This temperature control system was employed in this work for providing a stable temperature control of the LC cells and the reference cells.

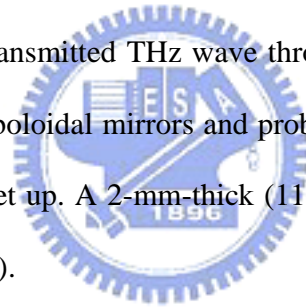


There are several absorption lines of water in the range of 0.2 to 1.5 THz [27]. We found that those water lines will affect the accuracy of the measured results. According to this, a dry environment is necessary for obtaining accurate results. We used acrylic plates to make a box, which covers whole THz system to approach a close system. The dry nitrogen gasified from liquid nitrogen was employed to purge and 3% of the relative humidity was achieved by continuously purging for 20 minutes. The system keeps being purged during measurement in order to retain the low humidity as 3%. The THz time domain signals and the spectra before and after purging are shown in Fig. 2.3.2.3 (a) and (b), respectively.

2.4. Experiment

2.4.1. Focusing beam system

The time-domain spectroscopy experimental setup shown in Fig.1.2.2.1 is similar to the conventional one and has been described in Sec.1.2.2. Briefly, a mode-locked Ti: Sapphire laser ($\lambda=800$ nm) generating ~ 35 fs pulses at a repetition rate of 80 MHz with 400 mW average output power is used as the light source. The laser beam is divided into two beams, a pump and a probe. A large-aperture photoconductive antenna is used as a THz emitter in our THz spectrometer. The antenna was made from an arsenic-ion-implanted- GaAs wafer with two AuGe electrodes separated by about 2 mm. It was biased at about 800 V. The pump beam illuminates the area between the two electrodes with focused ultrashort laser pulses to produce synchronous bursts of THz wave. The THz wave is collimated and focused on the sample by a pair of off-axis paraboloidal mirrors. The transmitted THz wave through the sample is collimated by a second pair of off-axis paraboloidal mirrors and probed by the delayed probe beam and the electro-optic sampling set up. A 2-mm-thick (110) ZnTe crystal is used for sensing the THz wave (see Sec.1.2.2).



2.4.2. Collimated beam system

In order to approach the calculation model mentioned in Sec.2.2.2 for extracting the optical constants, we also establish an antenna-based THz TDS system with a collimated beam. The sketch of this system is shown in Fig. 1.2.1. Briefly, the linear polarized THz pulses generated by femtosecond-laser excited dipole-type antenna fabricated on low-temperature-grown GaAs (LT-GaAs) are collimated by an off-axis paraboloidal mirror, and pass through the sample at normal incidence. The transmitted THz pulses are focused on another dipole-type antenna gated by time-delayed probe

pulses and oriented to detect THz waves polarized parallel to the incident THz wave polarization. The THz beam size is about 2.0-cm-diameter.

2.5. Results

In this section, we only report the results from the collimated beam system with nitrogen purging. Since the results are more accurate comparing to the results from the focusing system without drying the system. The issues of THz beam type and the humidity will be discussed later. In this section, we focus on the measurement of 5CB in order to give a continuous and complete report. The optical constants of another general LCs, E7, have also measured by focusing beam system and will be shown and discussed in Sec.2.6.

2.5.1. Time-domain signals

The time domain signals passing through the reference cell and the LC cell were measured by the THz TDS-system with the collimated THz beam. The system was purged by nitrogen in order to remove the water vapor on the path of the THz beam. The THz waves pass through the reference cell and LC cell (filled with 5CB) normally. The e-ray and o-ray of THz waves are defined by the linear polarization of THz wave, which parallel and perpendicular to the aligned direction of LC cell, respectively. Figure 2.5.1.1 (a) and (b) show the measured time domain signals of THz waves, which pass through the reference cell, LC cell with e-ray (Fig. 2.5.1.1(a)) and LC cell with o-ray (Fig. 2.5.1.1(b)) at 25 °C. The signals passing through the LC cell show clear time delay from the reference signal. There are also tiny difference of intensities appeared between these three signals, which might come from the absorption or the different Fresnel reflective loss from the different condition of the LC-quartz interface. After applying the

FFT to the signals, the frequency and the phase spectra can be obtained. The complex optical constants of LC can be extracted through the mentioned numerical method (Sec.2.2.2) by comparing the LC signal and reference signal. The extraordinary and ordinary indices were calculated separately.

By looking at the full time domain signals, there is a relatively small signal, which is the interface reflection of THz wave from the fused quartz substrates following after main THz pulse. Since the reflective signal isn't considered in the numerical analysis, we cut the signal right before the reflective signal. Because that the main (first) THz signal goes to zero before the reflective signal, the cutting seems reasonable and acceptable and also let the calculation become simple. That is also the principle reason to purge the system.

2.5.2. Frequency dependence

The power and the phase spectra of the THz wave passing through the LC cell and reference cell can be obtained by applying FFT to the time domain signals. By comparing the spectra through the program we built (appendix B), the frequency dependently refractive indices will be extracted out. Because of the aligned LC layer can be treated as a uniaxial crystal, the o-ray and e-ray will see the different optical constants of LC, ordinary and extraordinary indices. The n_o , n_e , κ_o and κ_e are the real part and imaginary part of the optical constants of 5CB at 25 °C shown in Fig. 2.5.2.1. The circles and the open circles are the extraordinary and ordinary indices respectively. The real part of the indices shows clear anisotropy between n_e and n_o about 0.20 ± 0.02 . The imaginary part doesn't show clear anisotropy, which should be considered that the

LC layer is relatively thin to the wavelength of THz waves, which will be discussed in Sec.2.6.3. The imaginary indices run in the range of 0-0.02 from 0.20 THz to 0.95 THz. In this frequency range, there is no any resonant absorption appearing for 5CB. We repeated the measurement with different temperature setting at 27°C, 29°C, 30°C, 31°C, 32°C, 33°C, 33.5°C, 34°C, 34.5°C, 34.6°C, 36°C, 38°C and 40°C. The clearing point (nematic-isotropic phase transition) is found at 34°C. The real part of the indices in the temperature range of 25°C -35°C is shown in Fig. 2.5.2.2. The n_o and n_e increases and decreases in turns with the increasing temperature from 25°C to 35°C, which the behavior is the same with it in visible range [27].

2.5.3. Temperature dependence

The particular temperature dependence of LC is important both for the fundamental study and further applications, which is well known in the visible range [4]. In this part, we show the temperature dependence of 5CB in several fixed frequencies of 0.187, 0.219, 0.250, 0.281, 0.312, 0.344, 0.375, 0.406, 0.437, 0.469, 0.500, 0.531, 0.562, 0.593, 0.625, 0.656, 0.687, 0.716, 0.750, 0.781, 0.812, 0.843, 0.875, and 0.906 THz. A formula is defined here as a function of temperature for fitting. This equation doesn't have any physical meaning but provide a convenient way to deduce the indices with known frequency and temperature, which is given as [28]

$$n = A \times (B - T_R)^C, \quad (2.5.3.1)$$

where n is the refractive index and T_R is the reduced temperature, which is the difference between measured temperature and measured clearing point ($T - T_C$). A , B and C are the parameters, which are employed for fitting the measured data. The fitting parameters are shown in Table 2.5.3.1. The temperature dependences of the index of

5CB are shown in Fig. 2.5.3.1 with the fitting results. The circles and the open circles are n_e and n_o respectively. The aligned 5CB becomes isotropic when the temperature is higher than the transition temperature, which is also shown in Fig. 2.5.3.1 by stars. Below the transition temperature, the line show the average indices of n_e and n_o with $\frac{2n_o + n_e}{3}$ from fitting results.

2.5.4. Birefringence and order parameter

The birefringence of aligned LCs is the difference between n_e and n_o and also relates to the order parameter of LC molecules. Generally, the birefringence of LCs is the function of the temperature. The relation between can be described as $S = (1 - \frac{yT}{T_c})^\beta$ and $\Delta n \propto \rho^{1/2} S$, where the S is the order parameter, T is the temperature, T_c is the transition temperature, ρ is the density of 5CB and y is the fitting parameter [27]. In this section, we show the temperature dependent birefringence of 5CB and also the order parameter of 5CB, which agrees with it in visible range.

Figure 2.5.3.1 shows the temperature dependent birefringence of 5CB at the frequencies of 0.187, 0.219, 0.250, 0.281, 0.312, 0.344, 0.375, 0.406, 0.437, 0.469, 0.500, 0.531, 0.562, 0.593, 0.625, 0.656, 0.687, 0.716, 0.750, 0.781, 0.812, 0.843, 0.875, and 0.906 THz. The birefringence of 5CB decreases with the increasing temperature. This can be explained by that the thermal rotational motion of the molecules of 5CB becomes more actively (disorder) when the temperature increases below transition temperature. In principle, the birefringence should drop to zero suddenly when the temperature is higher than transition temperature. In the measured results, there is still

some birefringence appeared, which can be considered that the 5CB molecules are in a mixture state of nematic-isotropic phase. The curves are the fitting results by using $\Delta n(T) = D \times (1 - \frac{E \cdot T}{T_c})^F$ where Δn is the birefringence of 5CB, T is the temperature, T_c is the transition temperature and the D, E and F are the fitting parameters. We can obtain the order parameter of 5CB from the fitting parameters as $(1 - \frac{E \cdot T}{T_c})^F$. The fitting parameters, E and F, are 0.2 ± 0.02 and 0.985 ± 0.01 , respectively, with the transition temperature of 34.5°C , which agree with that found in the visible range. The order parameter is the character of materials that means it should be a constant no matter in which frequency range is measured. The order parameter of 5CB people found is $(1 - \frac{0.98 \cdot T}{T_c})^{0.22}$, which our data well agrees with [27]. On another words, it shows that the birefringence we measured in THz range is reasonable and reliable.

2.6. Discussion

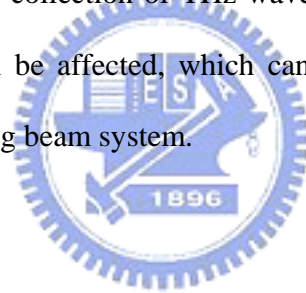
2.6.1. Comparison between focusing beam and collimated beam

Our earlier published results were measured by the focusing beam system without drying by purging mentioned in Sec.2.4 [30-32]. The measured method and the numerical process are similar to the collimated beam system. Briefly, the test cell was constructed as a double-cell with a liquid crystal cell and an empty reference cell side by side. Optical-quality fused silica windows were used as substrates. The thickness of the LCs is controlled by Mylar spacers. Homogeneous alignment of the nematic LC was achieved by rubbing the polyimide coated substrate. The temperature of the sample cell

was regulated within ± 0.1 °C. About the measured system, the sub-50fs pulse train from a mode-locked Ti: Sapphire laser (Spectra Physics Tsunami, $\lambda = 800$ nm) was divided into two beams, a pump and a probe. A large-aperture GaAs photoconductive antenna was used as the THz transmitter. The laser-excited THz wave was collimated and focused on the sample cell by a pair of off-axis paraboloidal mirrors. A 2-mm-thick (110) ZnTe crystal was used in an electro-optic sampling setup for coherent detection of the transmitted THz field in the time domain. Three sets of data for the real part of the refractive index of 5CB in the nematic and isotropic phases are shown in Fig. 2.6.1.1. The THz transmission measurements for 5CB in the nematic and isotropic phases were done at 25 °C and 38 °C, respectively. No sharp resonances, corresponding to absorption peaks, were observed in the frequency range from 0.3 to 0.8 THz. The real part of the refractive indices of 5CB in the nematic and isotropic phases, n_e , n_o and n_{iso} , all exhibit an rising trend with frequency. The values of n_{iso} fall between n_e and n_o , in good agreement with the relation, $n_{iso} = (n_e + 2n_o)/3$. We have also determined the extinction coefficients (the imaginary part of complex refractive indices) of 5CB. These are relatively small in this frequency range and are shown in Fig. 2.6.1.2. The frequency dependence of birefringence Δn of 5CB is shown in Fig. 2.6.1.3. It increases with frequency from 0.14 to 0.19. For comparison, the room-temperature ($T = 25^\circ\text{C}$) birefringence of 5CB measured in the visible ($\lambda = 633$ nm) is 0.18. In Figure 2.6.1.4 (a), the THz-band extraordinary and ordinary refractive indices of E7 are shown. Clearly, E7 exhibits a positive birefringence ($n_e > n_o$), which is consistent with that in the visible range. There is no sharp resonance in the 0.2-1.2 THz range, in which n_e varies from 1.69 to 1.80, while n_o varies from 1.51 to 1.63. The birefringence of E7 is thus 0.12 to

0.21 for the same frequency range (see Fig. 2.6.1.4 (b)). The corresponding imaginary indices of E7 are relatively small (< 0.04 , see Fig. 2.6.1.4 (c)).

The rising of indices measured by the focusing beam system is considered from the incorrect consideration of the Fabry-Perot effect in calculation (see Sec. 2.2.2). In the calculation, we assume that the THz beam, which is near by the focal point is collimated or approximately collimated. If the effect isn't considered correctly, it will affect a rising indices with increasing frequency, which has been discussed in Ref.24. On the other hand, the substrates we used is 3-mm-thick fused silica, which will also horizontally shift the focal point of the second parabolic mirror (the one right before the sample). If it's the case, the collection of THz wave on the third parabolic mirror (the one right after sample) will be affected, which can explain that the larger extinction coefficients from the focusing beam system.



2.6.2. Humidity effect

Water vapor [29] has several resonant absorption line in the THz frequency range. It also manifests in the temporal signals as oscillations after the main signal (Fig. 2.3.2.3(a)). Figure 2.3.2.3 (b) shows the power spectrum after applying FFT to the signal in Fig. 2.3.2.3 (a). We can find several sharp absorptive lines during this range. In general, it's still fine if we record the temporal signals all the way until the signal goes to zero, only that it would take a long time.

In previous works we have demonstrated the measurement for refractive indices of several typical LCs, 5CB and E7 [30-32], but the fluctuation of measured value was large and the accuracy was not satisfactory. In those measurements, we choose the 3-

mm-thickness fused silica windows to be the substrates because their good transparency both in visible and THz region. The reflective signals from both substrates appear at about 10 ps after the main signal, which has oscillation tail until about 25 ps after because of the water vapor absorption. The reflective signals interfere with each other and make the case more complex than what we discussed above. If we cut the signal before the first reflective signal, we will lose some information, which causes the inaccurate results. To demonstrate the humidity effect on the measured indices of refraction, we have done the measurement with and without drying the system by collimated beam. The results are shown in Fig.2.6.2.1, with circles and open circles for the undried system and the dash and dot lines for the dried system while keeping all the other conditions the same. The measured indices without drying slightly go up with higher frequency and the birefringence is roughly the same (~ 0.20).

If we want to treat the LC sample as an optically thin model, the reflections from substrates should be removed. There are two ways to go: we can let the substrates as thick as possible, or we can cut down the oscillation in the first directly transmission of the THz wave by removing the humidity on the all path of the THz waves.

2.6.3. Error analysis

The optical constants of LCs in the range of GHz to THz interest people because of the value on both fundamental research and applications. Several groups have investigated it mentioned in Sec. 2.1. In THz frequency range, Nose *et al.* have demonstrated that the ordinary and extraordinary refractive indices of 5CB are $1.819+0.0578i$ and $2.02+0.06i$ at 0.69THz , $1.937+0.0221$ and $2.306+0.0046i$ at 1.40THz and $2.115+0.0379i$ and $2.28+0.0159i$ at 2.54THz , which our data slightly disagree with.

The accuracy of the measured indices can be confirmed by checking all the error sources such as (in our case) system fluctuation, calculation model, the accuracy of the thickness of the LC layer, aligned quality of the LC and the accuracy of the index of the substrates. We will discuss it one by one to give a idea of the possible errors.

In order to check the system fluctuation and stability, we did the following tests: measuring the repeatability of the temporal signals and measuring the well know material such as the fused silica in this frequency range [33]. For the repeatability test, we have measured the temporal signals several times with separating time of 5 minutes, which is shown in Fig. 2.6.3.1. The signals repeated quite well on time domain (<0.01 ps). We have also compared the phase and power spectra to each other, shown in Fig. 2.6.3.2; the power spectra of the two THz signals recorded at different time are shown in Fig. 2.6.3.2 (a) and the difference between phases of these two signals is shown in Fig. 2.6.3.2 (b). The tests show that both the power and the phase have very small fluctuation in the frequency range of 0.2–1 THz during the measurement. The phase fluctuation ($<5^\circ$) from the instability of the optic components is much less than the predicted phase difference from LC cell ($\sim 530^\circ$). The measured frequency dependent refractive indices of the fused silica at room temperature is $1.951 - 0i$ without dispersion in the range of 0.2-1.5 THz (Fig. 2.6.3.3), which agrees with that in literature [33]. The case of the LCs is more complicate than the single plate because two more substrates are employed for confining and alignment.

About the LC sample part, all the thickness of the LC layer, the alignment quality of LC molecules and the purity of LC will affect the indices. The thickness is measured by interference method, which can be accurate as $\pm 3\mu\text{m}$. On the other hand, if

all of the other errors are independent of the thickness of LC layer, the thicker the layer is, the more accurate results we can get. In reality, the LC layer has the limitation of the thickness due to the requirement of stable LC alignment. In our work (Sec. 2.5), a thickness of 260 μm was selected. The alignment quality of the 260- μm -thick cell can be checked by looking at the order parameter from the measured temperature dependent birefringence, which shows that the alignment is as good as it in a usual thin sample (see Sec.2.5.4). The pre-tilt angle of the LC cell is $1^\circ \sim 2^\circ$ [34]. The purity of LCs relates to the clearing point (nematic-isotropic phase transition) directly. The clearing point goes down with the increase of the impurity. The clearing point of 5CB in our work was found to be 34.5 $^\circ\text{C}$, which is very close to the ideal one ($<35^\circ\text{C}$) [27]. We also measured a 2.0-mm-thick 5CB sample by dried collimated beam system at 38 $^\circ\text{C}$ in isotropic phase. The results for real and imaginary indices of refraction are shown in Fig. 2.6.3.4. The real index runs from 1.64 to 1.61 in the range of 0.2-1.2 THz that is roughly equal to $\frac{2n_o + n_e}{3}$, where n_o and n_e are shown in Fig. 2.5.3.1.

2.7. Summary

In summary, we have investigated the far-infrared optical constants of several liquid crystals, 5CB and E7, using THz time-domain spectroscopy. Two THz TDS systems, focusing beam and collimated beam, were used in this work. By using focusing beam system, the optical constants of 5CB and E7, have been measured. The positive birefringence of these three LCs was observed, i.e., $n_e > n_o$, throughout this range and as high as 0.15 to 0.21, which is comparable to that in the visible rang. The absorption of them in the frequency range of 0.2 to 0.8 THz range is relatively small (<0.02). The

frequency dependence and temperature dependence of 5CB have been also reported completely by using collimated beam system. The system is dried by purging nitrogen down to 3% of relative humidity because of the absorption lines of the water vapor in THz range.

The results from two different systems, focusing beam and collimated beam, are also compared to each other and discussed. The increasing indices of liquid crystals, 5CB and E7, with increasing frequency measured from focusing beam system were found because of the incorrect consideration of the Fabry-Perot effect. The accurate optical constants of 5CB have been measured from collimated beam system. The frequency dependent results are shown in Fig. 2.5.2.1 and Fig. 2.5.2.2. In the frequency range of 0.2-1 THz, 5CB doesn't show any resonant absorption and clear dispersion. The ordinary and extraordinary indices of 5CB are 1.577 – 1.597 and 1.762 – 1.786, respectively. The extinction coefficient is smaller than 0.02 without anisotropy. The temperature dependence of 5CB has also reported, shown in Fig. 2.5.3.1, which the behavior is quite similar to it in visible range. The temperature dependence, which relates to the order parameter has also been reported and shown in Fig. 2.5.4.1. The order parameter is the character of materials, which should be fixed no matter measured in which frequency range. This is confirmed by fitting the results of temperature dependent birefringence. The error analysis has been discussed in Sec.2.6.3.

Bibliography

1. R. Chang, *Mater. Res. Bull.* **7**, 267 (1972); *Mol. Cryst. Liq. Cryst.* **30**, 155 (1975).
2. R. A. Soref and M. J. Rafuse, *J. Appl. Phys.* **43**, 2029 (1972).
3. W. Haase and D. Potzsch, *Mol. Cryst. Liq. Cryst.* **38**, 77 (1977).
4. E. G. Hanson and Y. R. Shen, *Mol. Cryst. Liq. Cryst.* **36**, 193 (1976).
5. E. Miraldi, C. Oldano, L. Trossi, and P. T. Valabrega, *Appl. Opt.* **21**, 4163 (1982).
6. S. T. Wu, U. Efron, and L. V. Hess, *Appl. Phys. Lett.* **44**, 1033 (1984).
7. I. C. Khoo, R. R. Michael, and G. M. Finn, *Appl. Phys. Lett.* **52**, 2108 (1988).
8. P. Joffre, G. Illiaquer, and J. P. Huignard, *Proc. SPIE* 1126, **13** (1989).
9. S. T. Wu, J. D. Margerum, H. B. Meng, C. S. Hsu, and L. R. Dalton, *Appl. Phys. Lett.* **64**, 1204 (1994).
10. K. C. Lim, J. D. Margerum, A. M. Lackner, L. J. Miller, E. Sherman, and W. H. Smith, *Liq. Cryst.* **14**, 327 (1993).
11. K. C. Lim, J. D. Margerum, and A. M. Lackner, *Appl. Phys. Lett.* **62**, 1065 (1993).
12. F. Guérin, J. M. Chappe, P. Joffre, and D. Dolfi, *Jpn. J. Appl. Phys.* **36**, 4409 (1997).
13. T. Nose, S. Sato, K. Mizuno, J. Bae and T. Nozokido, *Appl. Opt.* **36**, 6383 (1997).

14. F. Yang and J.R. Sambles, *Appl. Phys. Lett.* **81**, 2047 (2001)
15. F. Yang and J.R. Sambles, *Liqu. Crys.* **30**, 599 (2003)
16. F. Guérin, J. M. Chappe, P. Joffre, and D. Dolfi, *Jpn. J. Appl. Phys., Part 1* **36**, 4409 (1997)
17. [K. C. Lim](#), [J. D. Margerum](#), and [A. M. Lackner](#), *Appl. Phys. Lett.* **62**, 1065 (1993)
18. K.C. Lim, J.D. Margerum, A.M. Lackner and L.J. Miller, *Liqu. Crys.* **14**, 327 (1993)
19. S.T. Wu, Birefringence dispersions of liquid crystals, *Phys. Rev. A* **33**, 1270, 1986.
20. M. Born and E. Wolf, *Principles of Optics*, (Pergamon, New York, 1980), Ch. 2.
21. S.T. Wu and C.S. Wu, *J. Appl. Phys.* **65**, 527, 1989.
22. U. Efron, J. Grinberg, P. O. Braatz, M. J. Little, P. G. Reif, and R. N. Schwartz, *J. Appl. Phys* **57**, 1356, 1985.
23. M. Morizono, *SID Dig.* **21**, 4, 1990.
24. L. Duvillaret, F. Garet, and J. Coutaz, *IEEE J. Sel. Top. Quantum Electron.* **2**, 739 (1996).
25. P. E. Gill, W. Murray, and M. H. Wright, *Practical Optimization*, Academic Press, New York, 1981.
26. T. J. Scheffer and J. Nehring, *J. Appl. Phys.* **48**, 1783 (1977).

27. Iam-Choon Khoo, *Liquid Crystals-Physical properties and nonlinear optical phenomena*, Wiley-Interscience, New York, 1995.
28. Martin van Exter, Ch. Fattinger, and D. Grischkowsky, *Opt. Lett.* **14**, 1128 (1989).
29. S. Brugioni, S. Faetti and R. Meucci, *Liq. Crys.* **30**, 927 (2003).
30. T.-R. Tsai, C.-Y. Chen, C.-L. Pan, R.-P. Pan, and X.-C. Zhang, *Appl. Opt.* **42**, 2372 (2003).
31. R.-P. Pan, T.-R. Tsai, C.-Y. Chen, C.-H. Wang, and C.-L. Pan, *Mol. Cryst. Liq. Cryst.* **409**, 137(2003).
32. C.-Y. Chen, C.-F. Hsieh, Y.-F. Lin, R.-P. Pan, and C.-L. Pan, *Opt. Express* **12**, 2625 (2004).
33. D. Grischkowsky, S. R. Keiding, M. van Exter, and C. Fattinger, *J. Opt. Soc. Am. B* **7**, 2006 (1990).
34. H.Y. Wu, *Alignment Properties of Liquid Crystals on Ion Beam Bombarded Polyimide films*, Thesis in Electrophysics, National Thiao-Tung University, 2003.



Figure

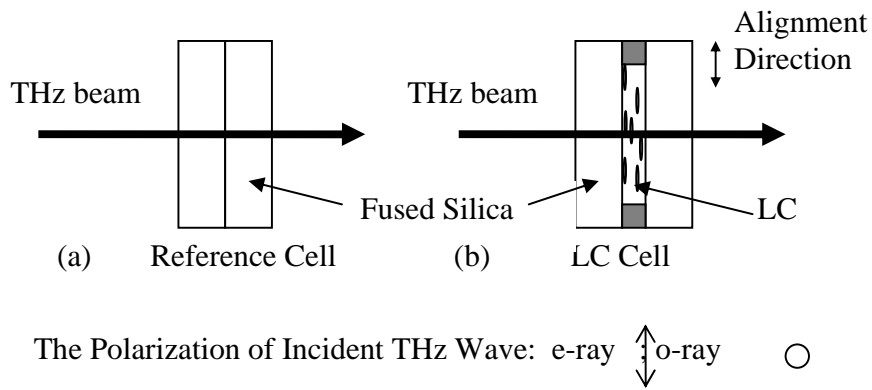


Figure 2.2.2.1 The sketches of reference cell (a) and the LC cell (b). The substrates are fused silica plates and the alignment of LC cell is homogeneous.



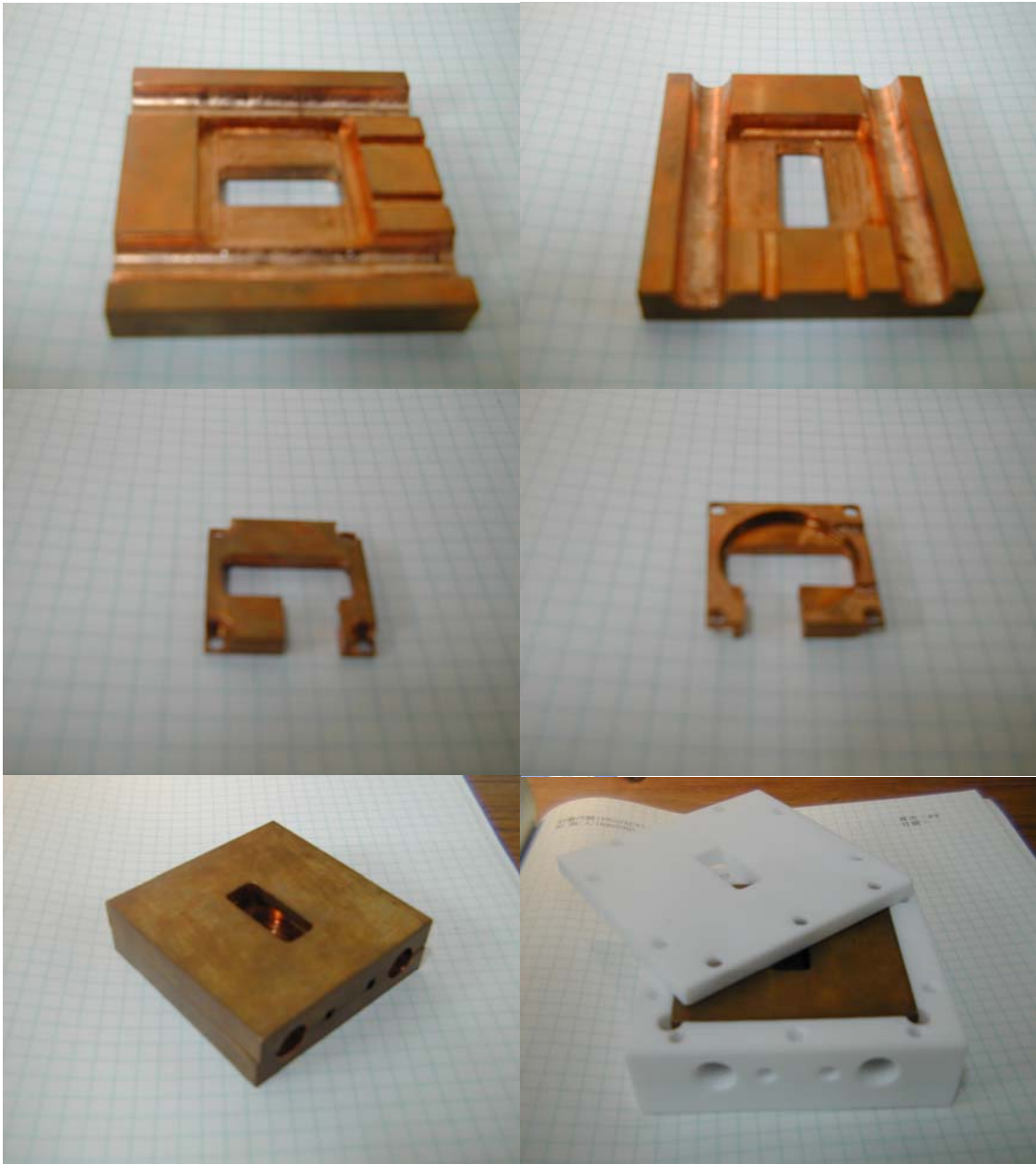


Figure 2.3.2.1 The pictures of the temperature-controlled sample holder, which consists with a copper oven (inside) and a Teflon cover (outside).

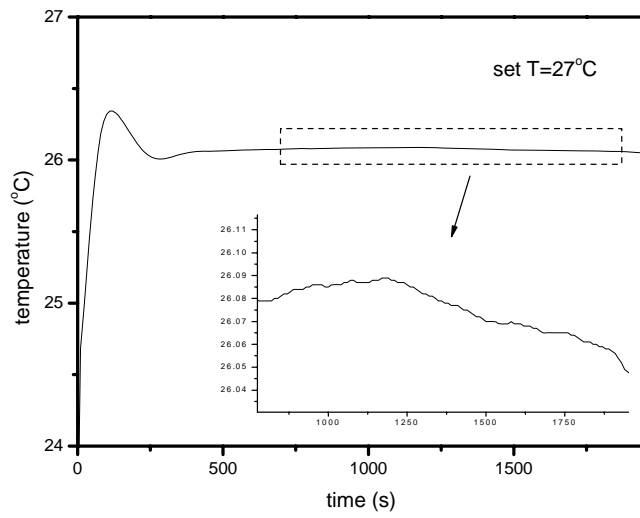


Figure 2.3.2.2 The testing result of the temperature control system. The inset shows a extended window from the dash frame.



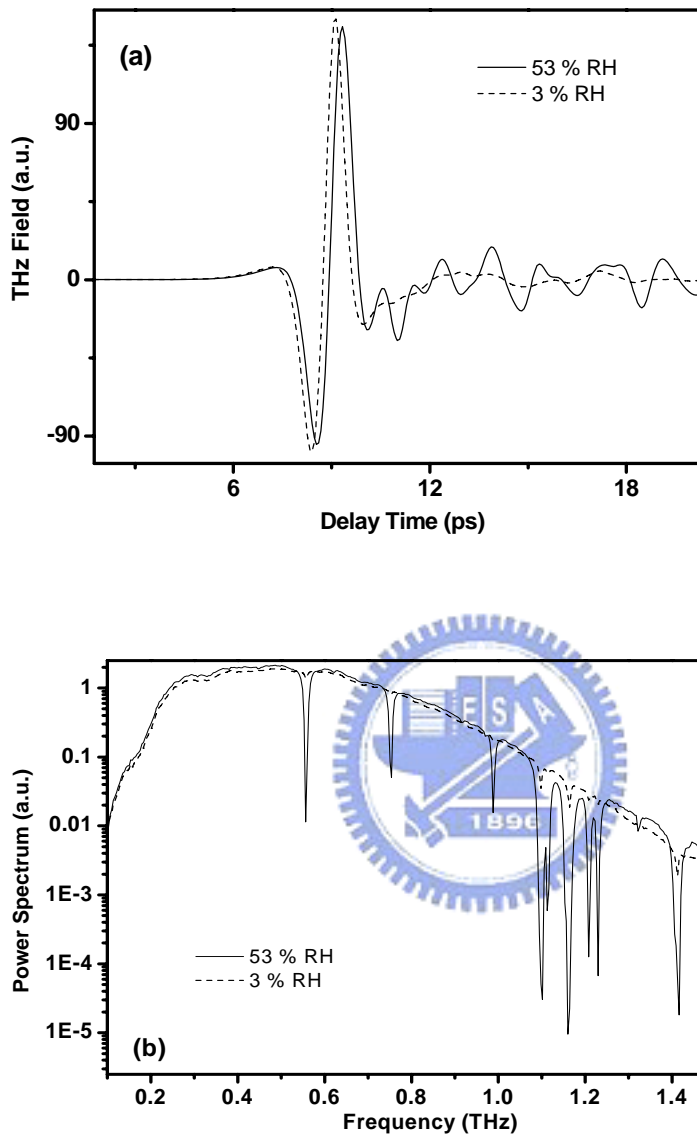


Figure 2.3.2.3 (a) The temporal profiles of the THz signals before (solid line) and after (dash line) purging. (b) The power spectra of the THz signals before (solid line) and after (dash line) purging. Several absorption lines of water vapor appear before purging. (RH: Relative Humidity)

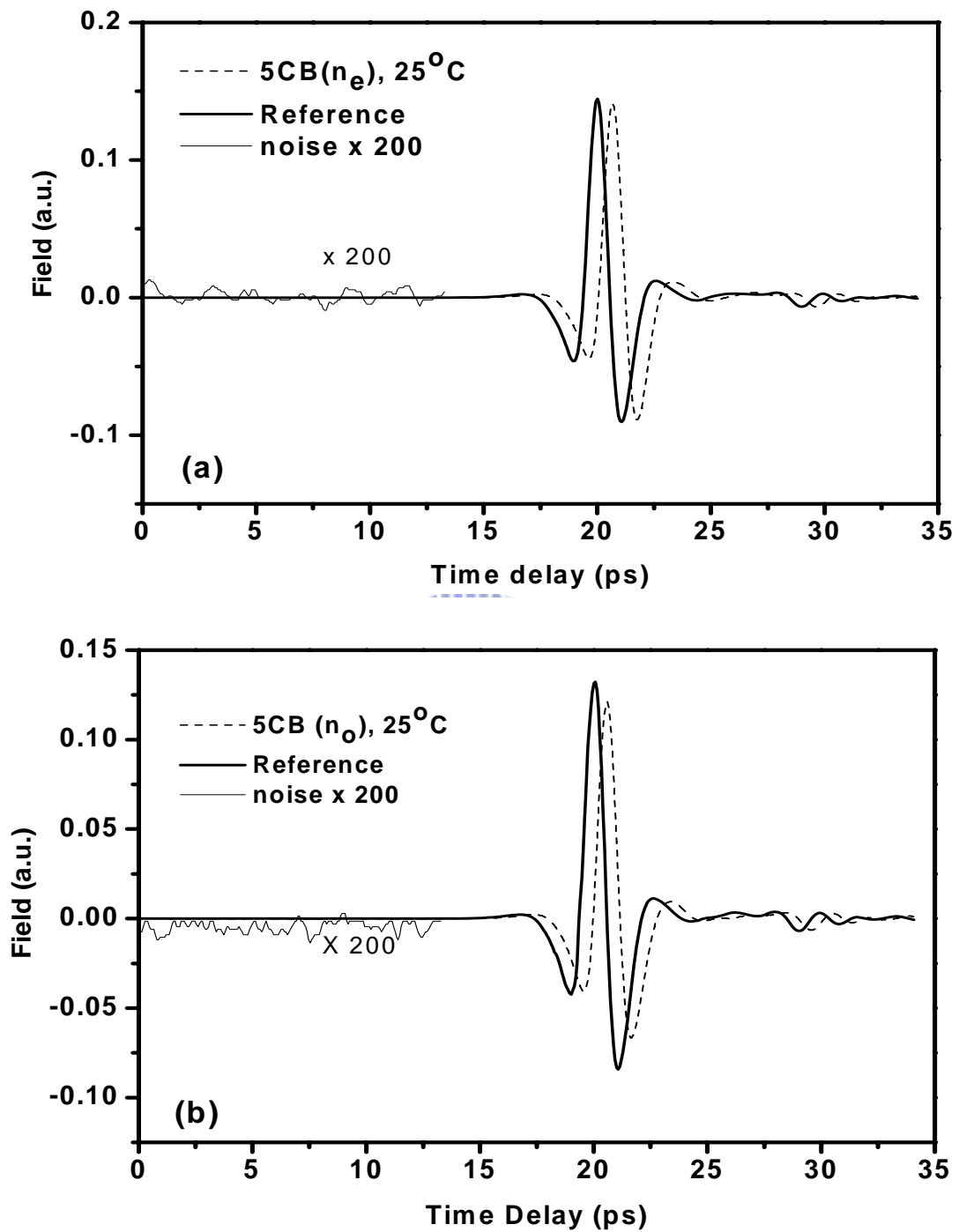


Figure 2.5.1.1 The measured time domain signals of THz waves, which pass through the reference cell, LC cell with e-ray (a) and LC cell with o-ray (b) at 25 °C.

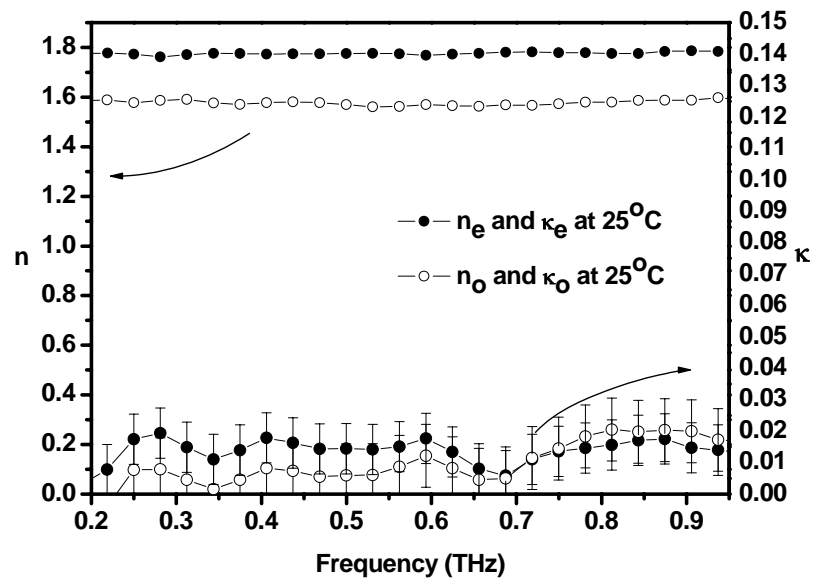


Figure 2.5.2.1 The n_o , n_e , κ_o and κ_e are the real part and imaginary part of the optical constants of 5CB at 25 °C. The circles and the open circles are the extraordinary and ordinary indices respectively.

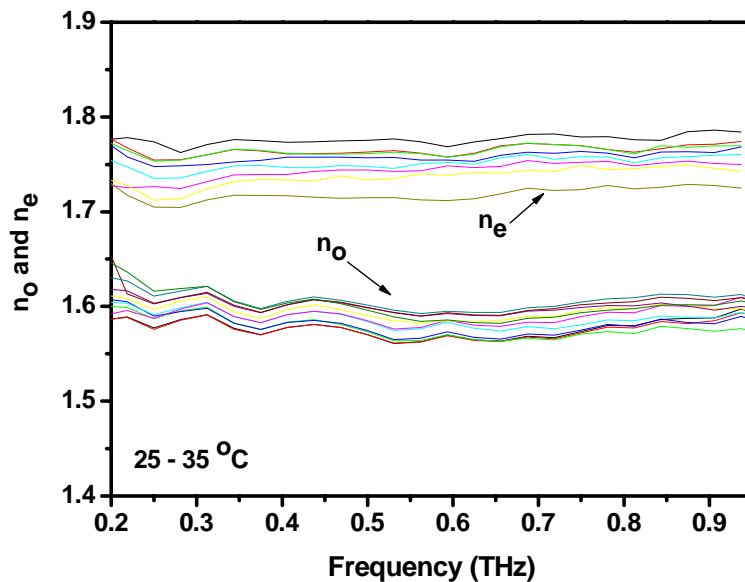
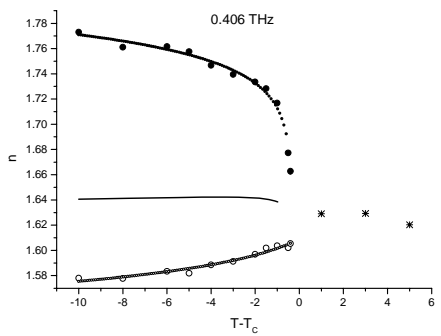
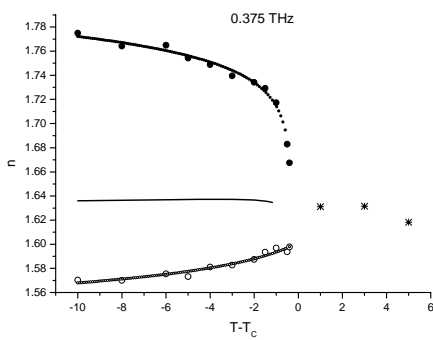
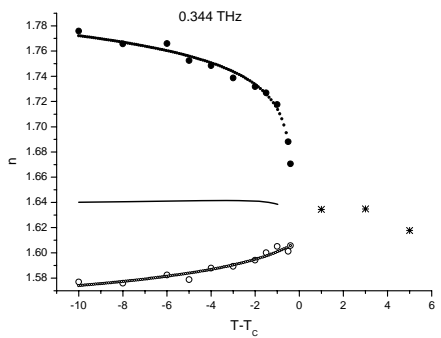
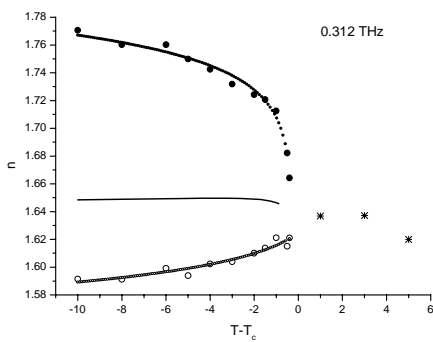
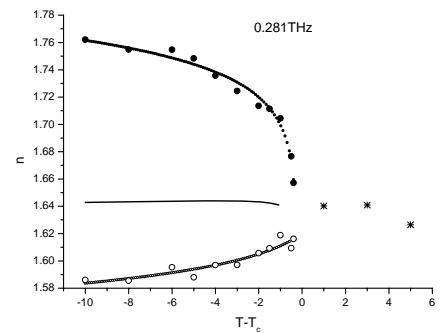
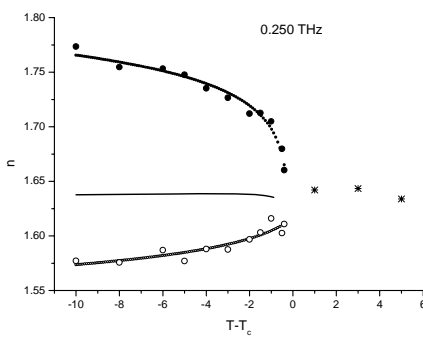
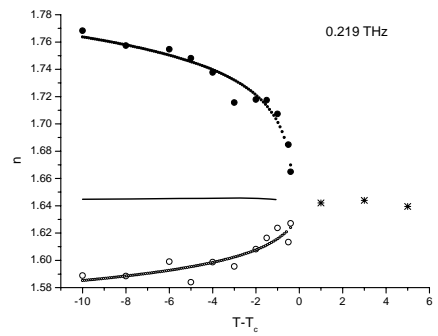
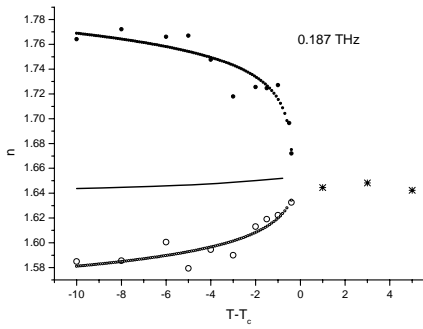
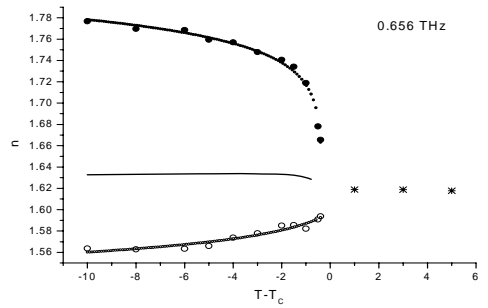
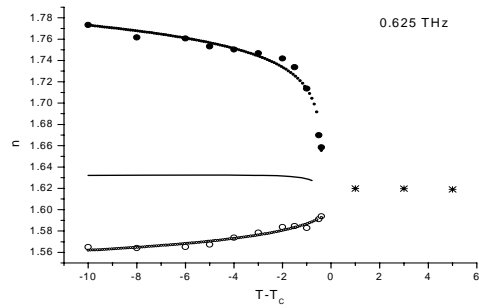
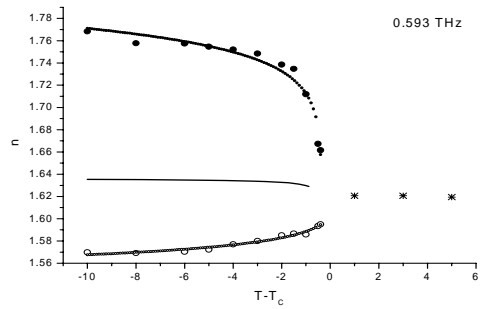
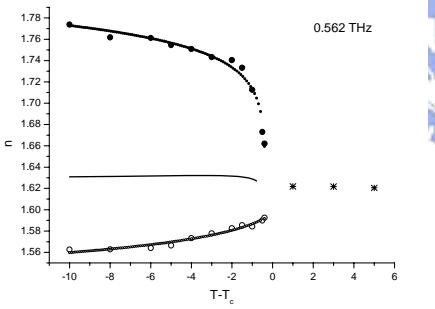
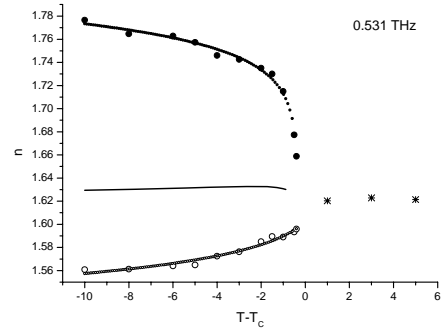
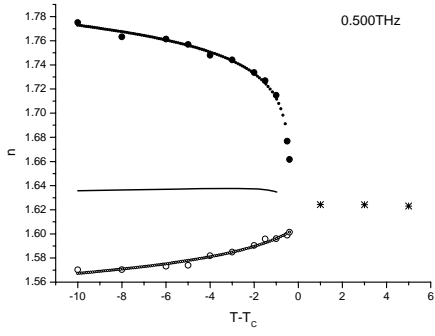
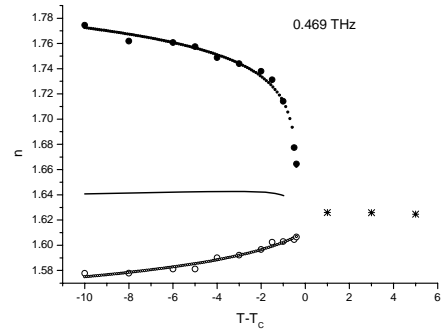
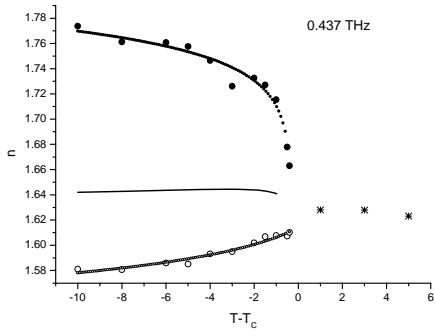


Figure 2.5.2.2 The real part of the indices in the temperature range of 25°C -35°C.





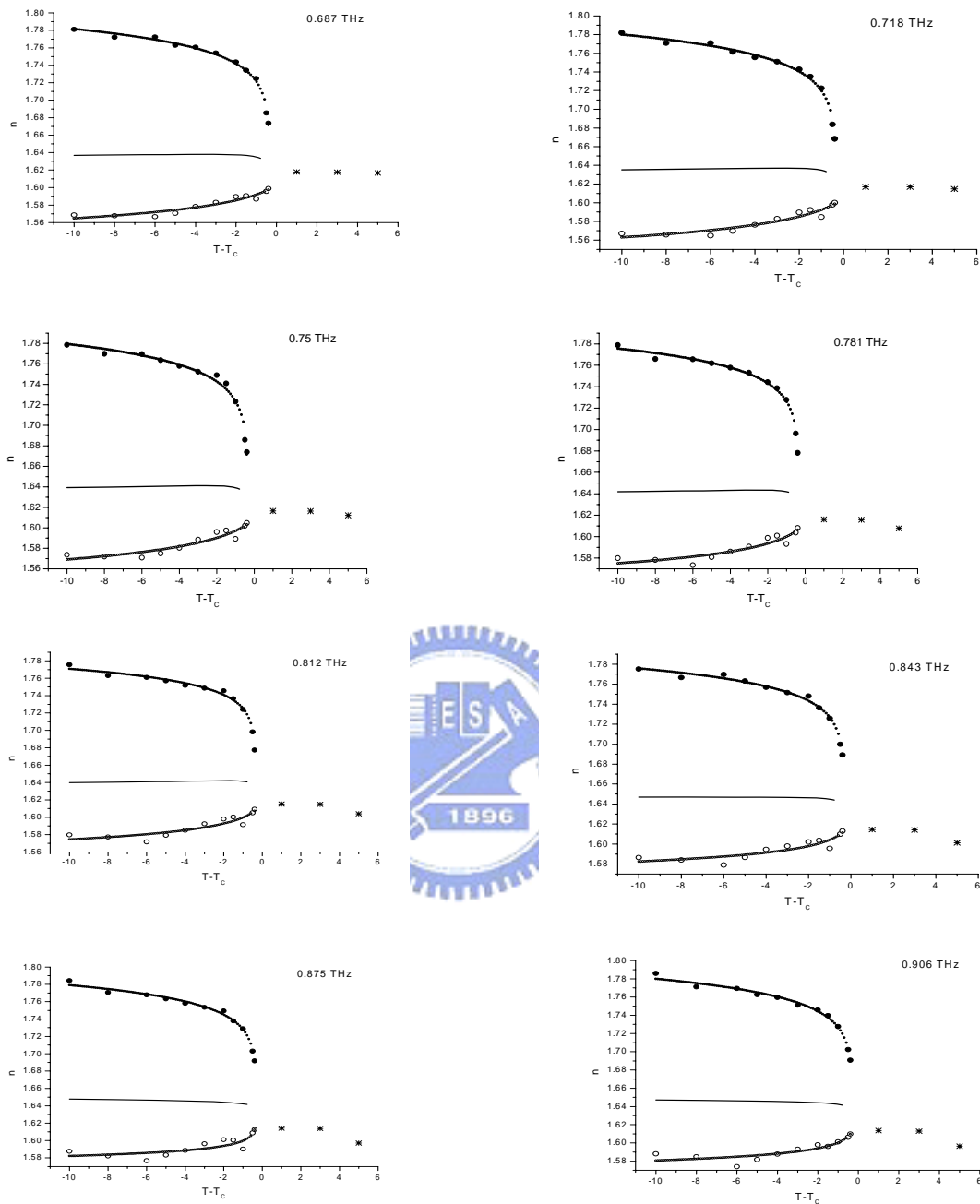
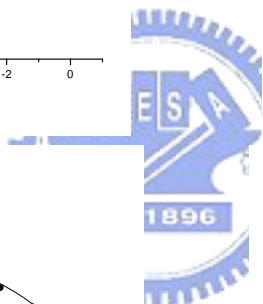
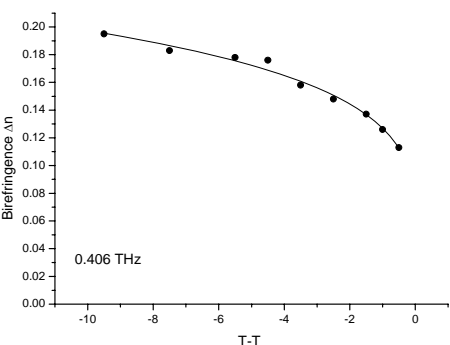
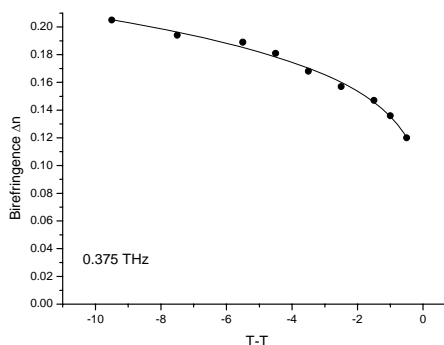
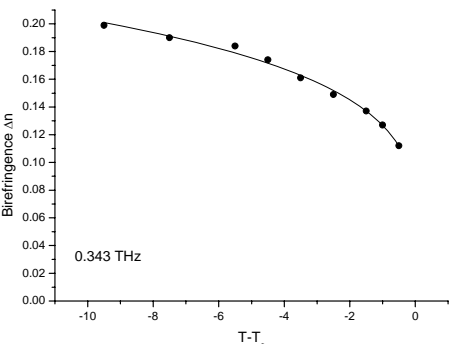
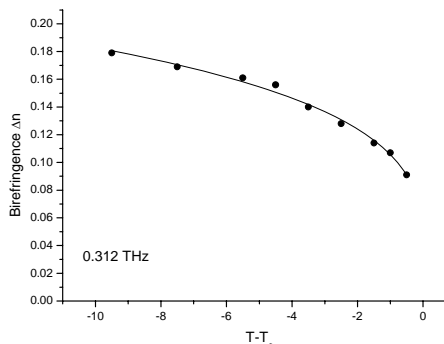
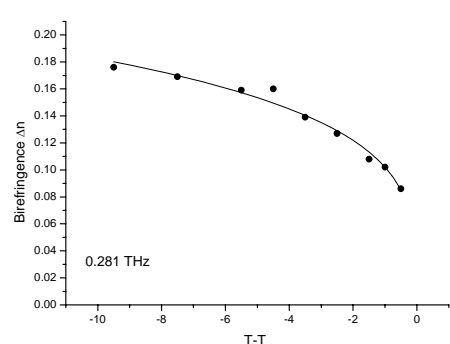
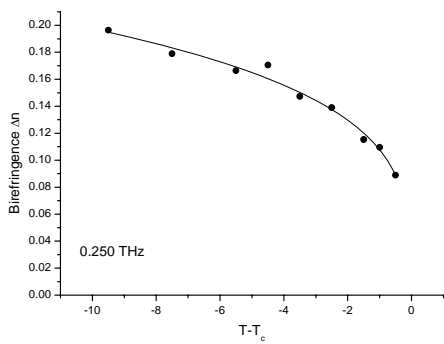
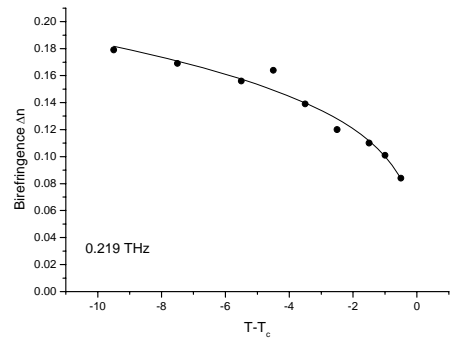
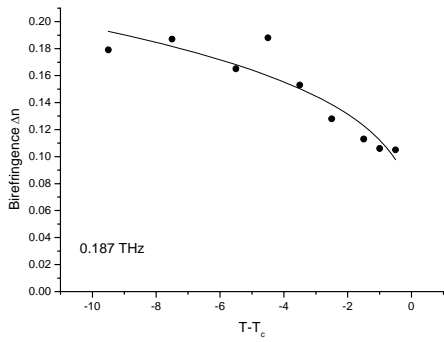
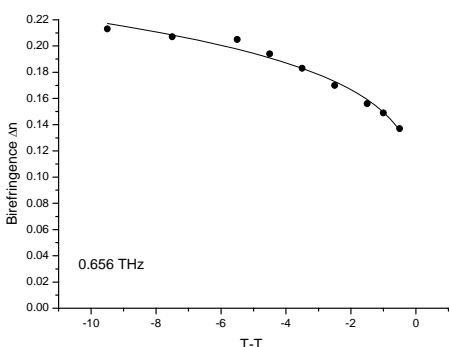
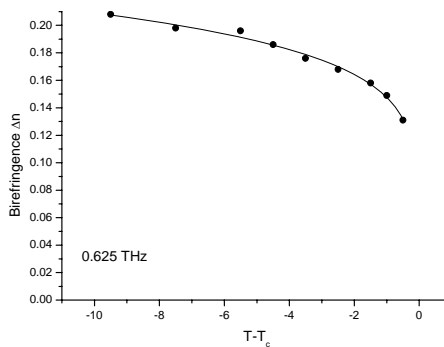
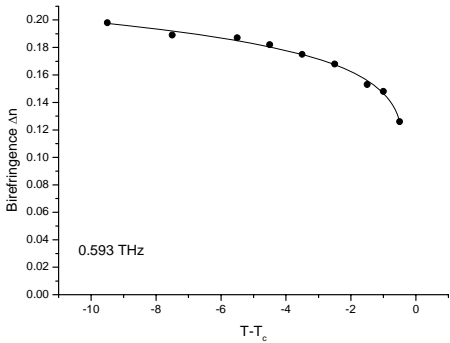
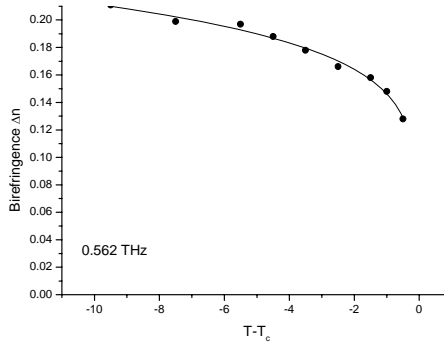
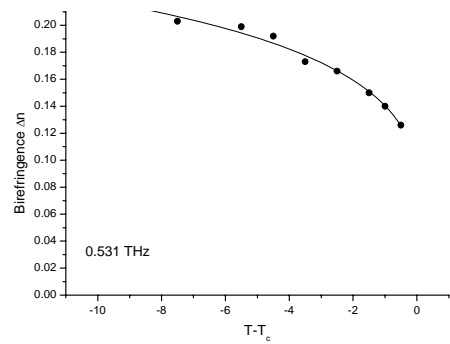
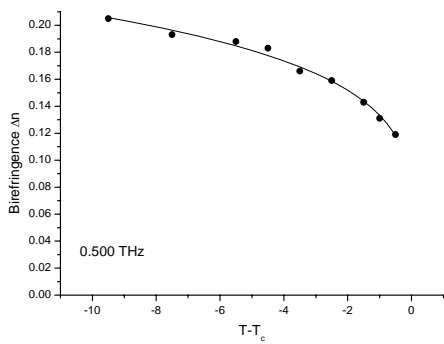
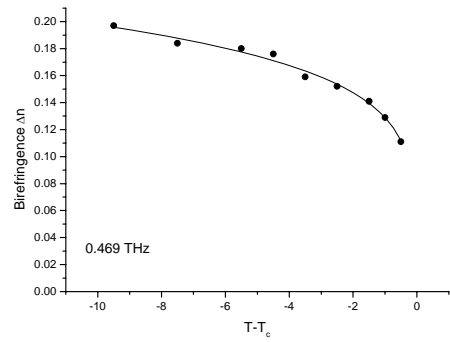
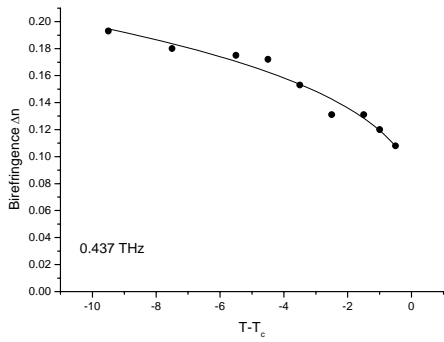


Figure 2.5.3.1 The temperature dependence of 5CB in several fixed frequencies of 0.187, 0.219, 0.250, 0.281, 0.312, 0.344, 0.375, 0.406, 0.437, 0.469, 0.500, 0.531, 0.562, 0.593, 0.625, 0.656, 0.687, 0.716, 0.750, 0.781, 0.812, 0.843, 0.875, and 0.906 THz. The circles and the open circles are the n_e and n_o , respectively and the stars are the index in isotropic phase. The solid lines are the average index of $\frac{2n_o + n_e}{3}$ at the temperature below T_c .





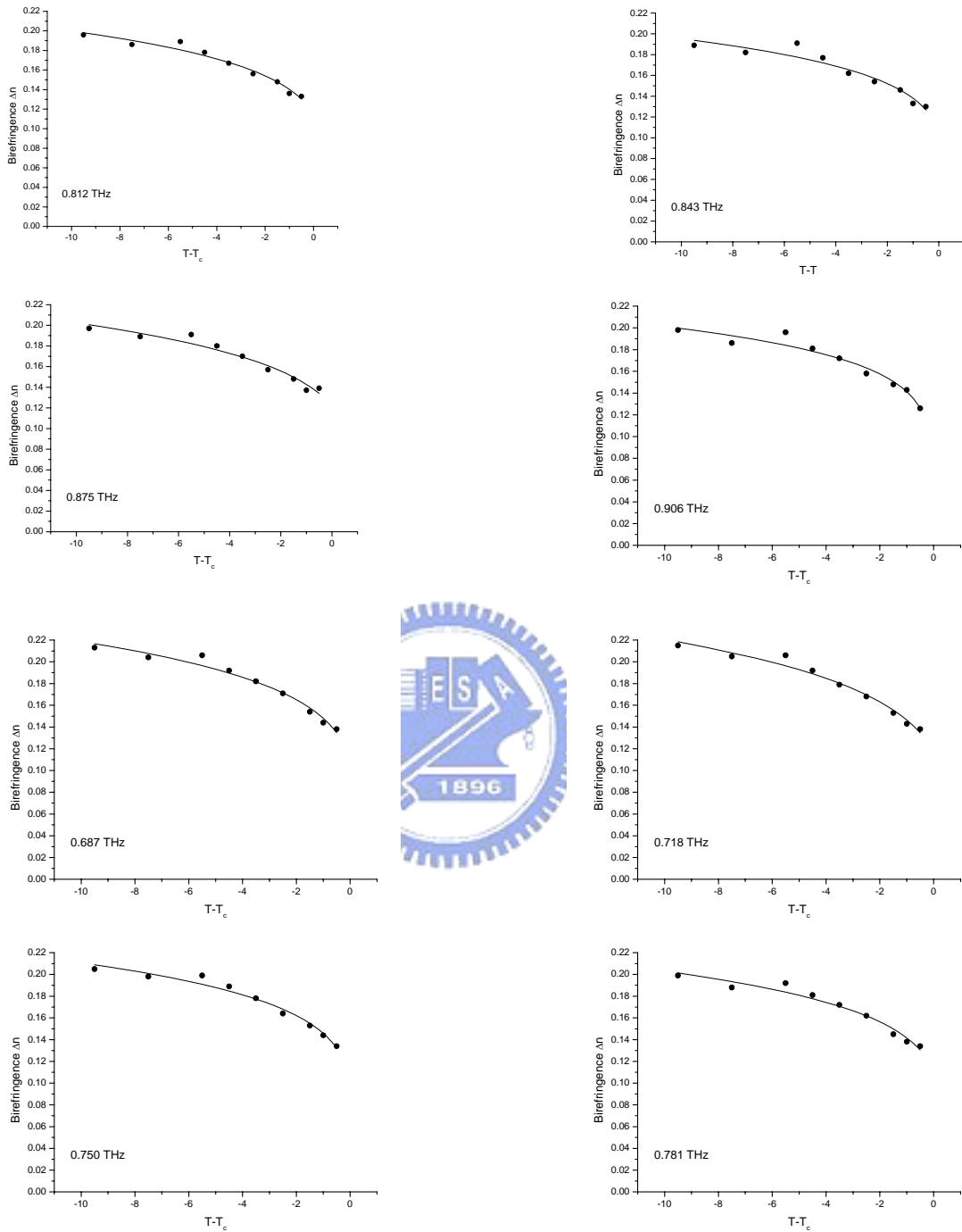


Figure 2.5.4.1 The birefringence of 5CB from Fig. 2.5.3.1. The curves are the fitting results.

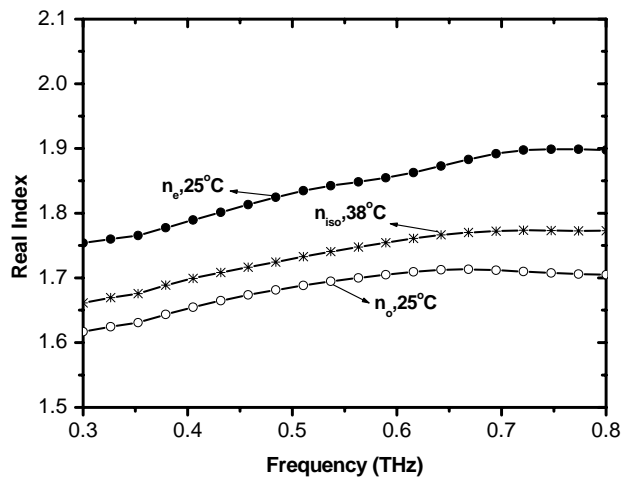


Figure 2.6.1.1 The frequency dependence of the real part refractive index of 5CB.

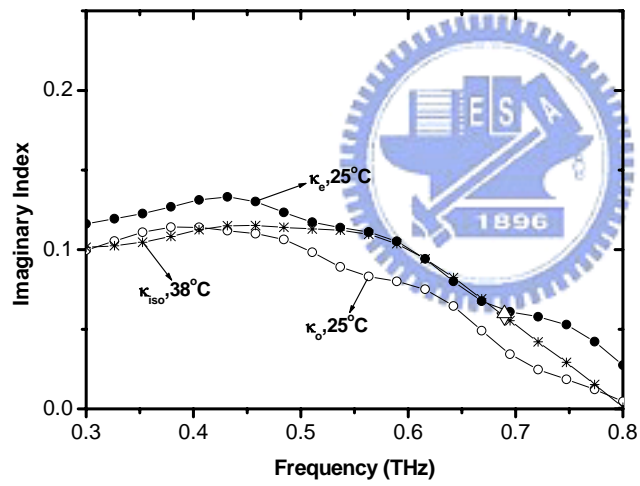


Figure 2.6.1.2 The frequency dependence of the imaginary part refractive index of 5CB.

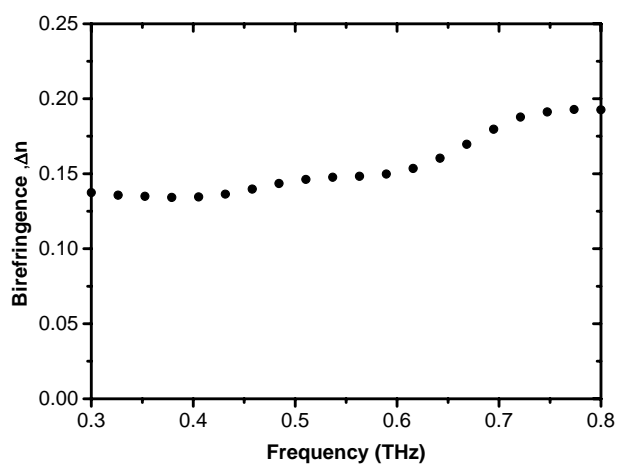


Figure 2.6.1.3 The frequency dependence of the birefringence of 5CB.



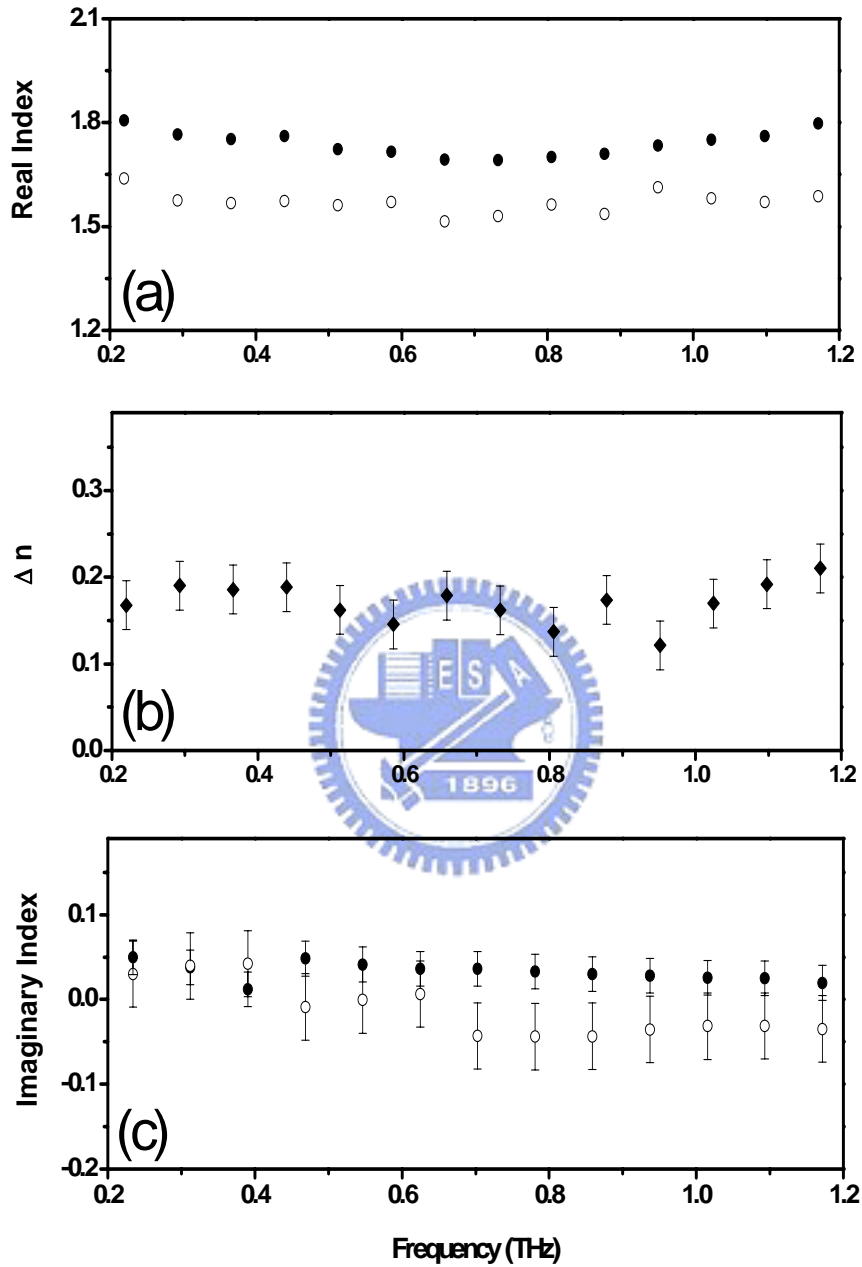


Figure 2.6.1.4 The room-temperature (a) extraordinary (red circles) and ordinary (blue circles) refractive indices, (b) birefringence, and (c) imaginary extraordinary (blue circles) and ordinary (red circles) refractive indices of E7 are shown as a function of frequency between 0.2 to 1.2 THz.

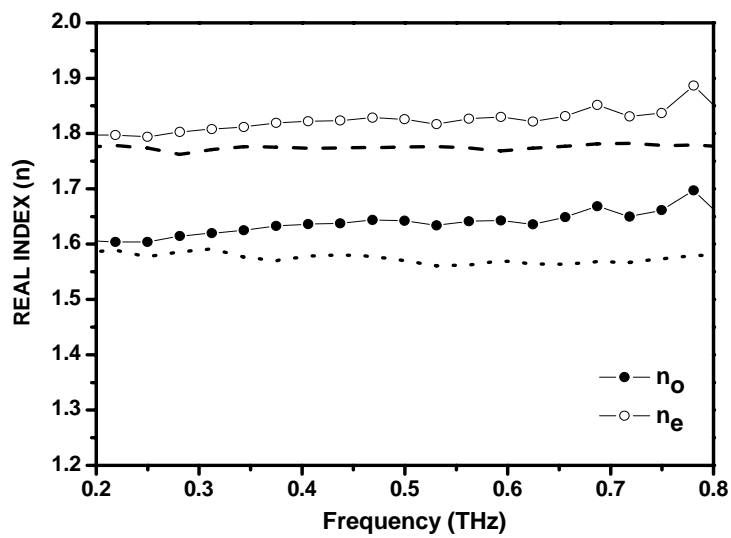


Fig. 2.6.2.1 The real index of 5CB measured by the THz-TDS system without drying. The THz beam passed through the sample is collimated beam and with normal incidence.

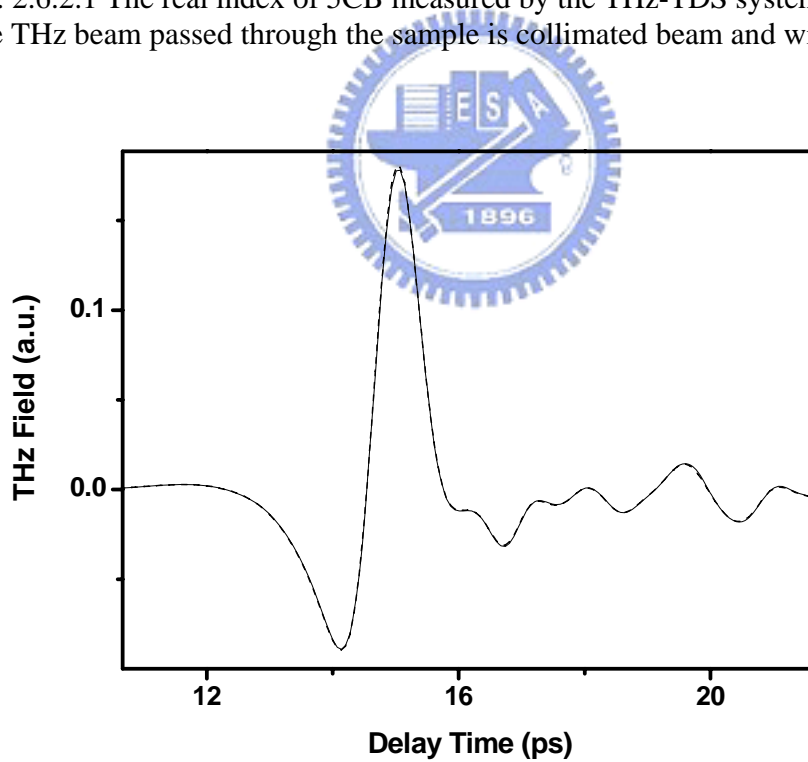


Figure 2.6.3.1 The temporal profiles of the THz signals recorded at different time for checking the repeatability.

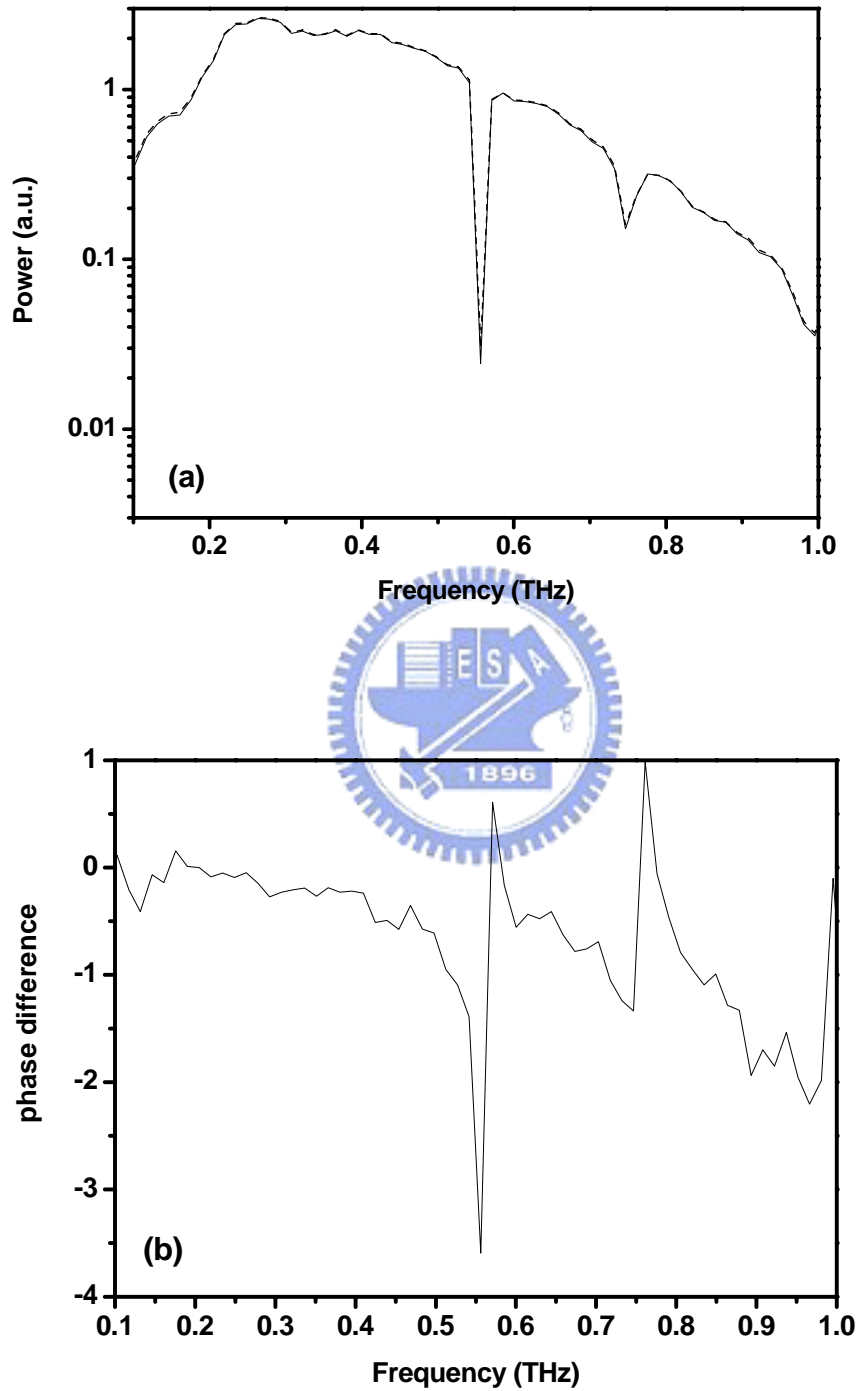


Figure 2.6.3.2 (a)The power spectra of the THz signals shown in Fig. 2.6.3.1. (b)The phase difference between two THz signals shown in Fig. 2.6.3.1.

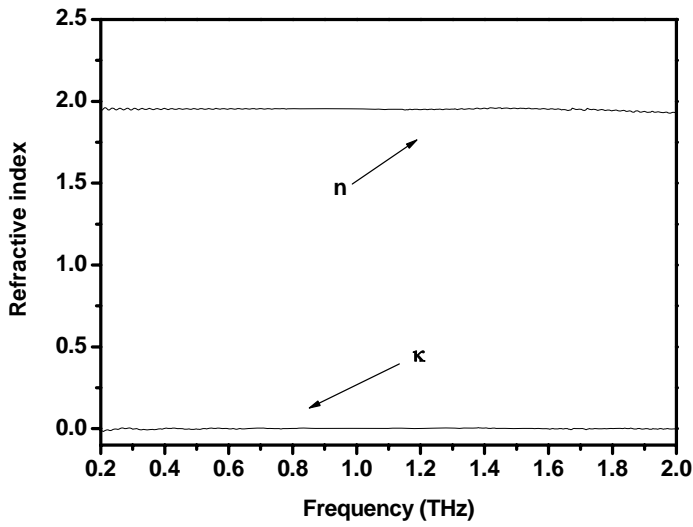


Figure 2.6.3.3 The measured refractive indices of fused silica in THz range.

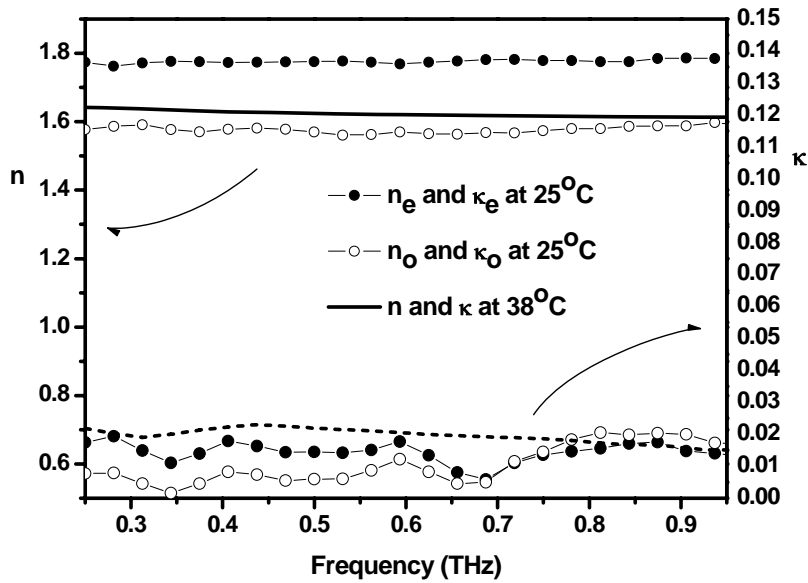


Figure 2.6.3.4. The complex optical constants of 5CB from 2-mm-thick cell measured in isotropic phase. The solid line and the dash line are the real and imaginary part respectively. The circles and open circles are the measured indices from thin sample, which have been shown in Fig. 2.5.2.1.

Table

frequency (THz)	A _o	B _o	C _o	A _e	B _e	C _e
0.219	1.706159	-0.17132	0.014533	1.621996	0.484098	-0.00975
0.25	1.702852	-0.15619	0.015851	1.619643	1.167518	0.01193
0.281	1.706969	-0.26922	0.013845	1.628633	1.583427	0.011444
0.312	1.715861	-0.30017	0.012951	1.632112	1.527217	0.010892
0.344	1.722044	-0.3057	0.012633	1.616452	1.434598	0.010921
0.375	1.722979	-0.33105	0.012397	1.610879	1.686762	0.011008
0.406	1.72177	-0.34356	0.012437	1.624173	2.162122	0.012189
0.437	1.719191	-0.32845	0.012778	1.632175	2.294422	0.013418
0.469	1.722941	-0.34257	0.012501	1.622331	1.814399	0.011993
0.5	1.721391	-0.33798	0.012982	1.612512	1.3994	0.011701
0.531	1.722375	-0.34891	0.012854	1.606205	1.239742	0.01275
0.562	1.722488	-0.34696	0.012718	1.601712	1.368953	0.010924
0.593	1.721763	-0.35248	0.012454	1.59174	0.361484	0.006557
0.625	1.722863	-0.35694	0.012667	1.594432	0.733914	0.008687
0.656	1.726522	-0.3429	0.013037	1.59944	1.123686	0.010336
0.687	1.730538	-0.33306	0.012803	1.603058	1.013795	0.010096
0.718	1.729269	-0.34355	0.012776	1.6032	0.89355	0.010688
0.75	1.732391	-0.35094	0.011828	1.607052	0.866241	0.010041
0.781	1.734336	-0.35963	0.010384	1.606057	0.586836	0.008263
0.812	1.732746	-0.36679	0.0096	1.602829	0.29201	0.007685
0.843	1.733756	-0.32094	0.010542	1.605666	0.169034	0.006281
0.875	1.734888	-0.2997	0.011057	1.597293	-0.29219	0.004213
0.906	1.733556	-0.28455	0.011629	1.599054	-0.13045	0.00506
0.937	1.728894	-0.15681	0.01326	1.600826	-0.28645	0.003455

Table 2.5.3.1 The fitting parameters of Eq. 2.5.3.1 mentioned in Sec.2.5.3.